Tunneling magnetoresistance induced by controllable formation of Co filaments in resistive switching Co/ZnO/Fe structures

2014 EPL 108 58004

(http://iopscience.iop.org/0295-5075/108/5/58004)

A Letters Journal Exploring the Frontiers of Physics

December 2014

EPL, **108** (2014) 58004 www.epljournal.org
doi: 10.1209/0295-5075/108/58004

Tunneling magnetoresistance induced by controllable formation of Co filaments in resistive switching Co/ZnO/Fe structures

Zhihuan Yang, Qingfeng Zhan[(a)], Xiaojian Zhu, Yiwei Liu, Huali Yang, Benlin Hu, Jie Shang, Liang Pan, Bin Chen and Run-Wei Li[(b)]

Key Laboratory of Magnetic Materials and Devices, Ningbo Institute of Material Technology and Engineering (NIMTE), Chinese Academy of Sciences (CAS) - Ningbo 315201, PRC and
Zhejiang Province Key Laboratory of Magnetic Materials and Application Technology, Ningbo Institute of Material Technology and Engineering (NIMTE), Chinese Academy of Sciences (CAS) - Ningbo, 315201, PRC

received 6 September 2014; accepted in final form 13 November 2014
published online 2 December 2014

PACS 85.75.-d – Magnetoelectronics; spintronics: devices exploiting spin polarized transport or integrated magnetic fields
PACS 73.40.Rw – Metal-insulator-metal structures

Abstract – We demonstrated that the formation of magnetic conductive filaments in Co/ZnO/Fe sandwich structures can be employed to produce a nanoscale magnetic tunnel junction (MTJ) and control the tunneling magnetoresistance (TMR). The pristine Co/ZnO/Fe structures with a 100 nm thick ZnO layer do not exhibit any remarkable TMR. Under voltage sweeps performed on the sandwich devices, Co conductive filaments were grown in a ZnO layer, which leads to the formation of nanoscale Co/ZnO/Fe MTJs and the occurrence of TMR. In addition, a sign inversion of TMR was found in the nano-MTJs by carrying out the further voltage sweeps or varying the measuring bias voltage, which could be well understood in terms of the resonant tunneling caused by impurity scattering in a ZnO barrier.

Introduction. – Over the last few decades, a variety of novel phenomena, such as resistive switching (RS) [1,2], tunneling magnetoresistance (TMR) [3–6], and giant magnetoresistance (GMR) [7–9], has been continuously discovered in thin-film sandwich structures. For example, an electrode/insulator/electrode sandwich structure can be reversibly switched between a high-resistance state (HRS) and a low resistance state (LRS) under externally applied electric fields, which is termed the RS effect and can be interpreted by the mechanisms based on conductive filament, charge trapping/de-trapping, thermochemical reaction, metal-insulator transition and other models [10,11]. On the other hand, in a magnetic tunnel junction (MTJ) where an ultra-thin insulating barrier is sandwiched between two ferromagnetic electrodes, a TMR ratio up to hundreds of percent could be achieved due to the spin-polarized tunneling of conduction electrons across the insulating barriers. For a spin-valve structure with a nonmagnetic conductive layer sandwiched between two ferromagnetic layers, a GMR ratio up to a few tens of percent could be obtained owing to the spin-dependent scattering of polarized conduction electrons at the interfaces. Due to the great potential for application in sensors and information storage devices, these achievements obtained in sandwich structures have received widespread attention [1–15].

Most of the previous investigations have separately focused on either the RS behaviours or the spin-dependent effects, but ignored the coexistence of these effects in a multilayered structure. Recently, in sandwich structures with ferromagnetic electrodes or barriers, both magnetoresistance and magnetization have been found to be electrically switched by means of the RS operations [16–22]. For example, Chen *et al.* demonstrated that, due to the variation of oxygen vacancies during the rupture and rejuvenation of oxygen-vacancy–based filaments, both the magnetization and the coercive fields of Pt/Co:ZnO/Pt structures can be significantly modulated by applying electric fields [20]. Halley *et al.* observed the different TMR behaviours for Fe/Cr/MgO/Fe MTJs in the LRS and HRS, and the migration of oxygen vacancies and atoms due to the strong electric field that develops across the insulating barrier were believed to be responsible for the electrical switching phenomena [21].

(a) E-mail: zhanqf@nimte.ac.cn
(b) E-mail: runweili@nimte.ac.cn

In a number of RS sandwich structures, when a positive voltage is applied to the electrochemically active electrode, metal atoms can be oxidized to ions. After traveling a short distance into the insulating layer, the ions will be reduced back to atoms and gradually form metal conductive filaments from the anode surface to the cathode layer [23,24]. By applying a sufficient negative bias voltage, the filament could be electrochemically dissolved, switching the device back to the LRS. A positive voltage lower than that used in the forming process would rejuvenate the previously ruptured filament segments. The formation, rupture, and rejuvenation of conductive filaments have been used to construct magnetic nanostructures and modulate their properties. Recently, Jang *et al.* found that, in Co/TaO_x/Cu/$Ni_{80}Fe_{15}Mo_5$ structures, the GMR behaviour appears in the LRS and vanishes in the HRS due to the rejuvenation and rupture of Cu spin transport channels in TaO_x, which leads to the formation and destruction of the GMR structure of Co/Cu/$Ni_{80}Fe_{15}Mo_5$ [22]. For a ferromagnet/insulator/ferromagnet sandwich structure, if the conductive filament is not connected to the cathode and the insulating layer in between is thin enough for the spin-polarized electron tunneling through it, a nanoscale MTJ is expected to be produced.

In this paper, we experimentally showed a new approach to construct nanoscale MTJs in Co/ZnO/Fe sandwich structures by controlling the growth of Co conductive filaments with electric fields. The positive and negative TMRs and the inversion of TMR with varying the measuring bias voltages were observed after different voltage sweeps performed on the devices, which can be interpreted based on the mechanism of resonant tunneling via impurity states located at the ZnO barrier.

Experiment. – Multi-layered films with a structure of, from the top side, Au(3 nm)/Co(100 nm)/ZnO(100 nm)/Fe(100 nm)/Au(100 nm), as schematically shown in fig. 1(a), were deposited on thermally oxidized Si substrates using a magnetron sputtering system with a base pressure below 1×10^{-4} Pa. Au layers were rf sputtered at an Ar pressure of 1 Pa at room temperature. Fe layers were dc sputtered with an Ar pressure of 0.2 Pa at an elevated temperature of 200 °C to reduce the surface roughness. ZnO layers were deposited by rf sputtering a ceramic ZnO target in 80%Ar/20%O_2 ambient of 1 Pa at room temperature. Co top electrodes with a diameter of 200 μm were dc sputtered in an Ar atmosphere of 0.2 Pa at room temperature. The films were capped by a 3 nm thick Au layer to avoid oxidation. The surface topography and the hysteresis loops were characterized at room temperature by the Atomic Force Microscope (AFM, SII Nanotechnology) and the Vibrating Sample Magnetometer (VSM, Lakeshore Model 668), respectively. The current-voltage (*I-V*) characteristics and magnetoresistance curves were measured at 10 K by using a semiconductor parameter analyzer (Keithley 4200) integrated with a cryogenic probe station (Lakeshore EMPX-HF). The temperature dependence of resistance was measured by using a physical-properties measurement system (PPMS, Quantum Design) with a constant dc current of 50 μA.

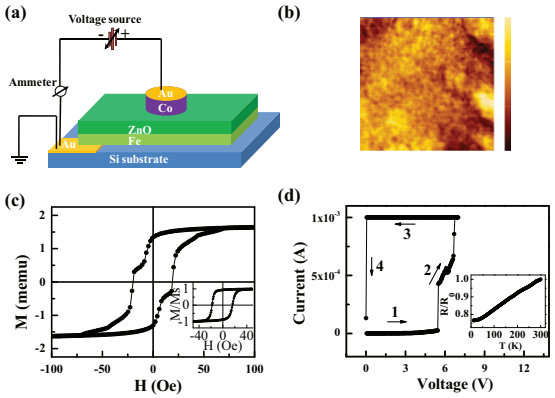

Fig. 1: (Colour on-line) (a) Schematic of the multi-layered resistive switching Co/ZnO/Fe structures. (b) AFM images ($1 \times 1\ \mu m^2$), where the colour contrast (dark to bright) for the height scale corresponds to 5.8 nm, and (c) hysteresis loop for the as-grown Co/ZnO/Fe structures. The hysteresis loop of a reference Fe film grown on a Si substrate is shown in the inset. (d) The *I-V* curve corresponds to the forming process of an as-grown cell under a voltage. The voltage sweep sequences and directions are marked with numbers and arrows. The temperature dependence of resistance for the cell in the LRS is shown in the inset.

Results and discussion. – Figure 1(b) shows the surface topography of the as-prepared Co/ZnO/Fe multilayer with a root-mean-square (RMS) roughness of 0.91 nm. As revealed in fig. 1(c), the hysteresis loop of the film exhibits a feature of two-step reversal due to the different coercivities of the Fe and Co layers. The hysteresis loop of a reference Fe film grown on a Si substrate, as shown in the inset of fig. 1(c), indicates that the sharp magnetic switching near 20 Oe corresponds to the Fe layer.

A voltage sweep of $0 \rightarrow 7 \rightarrow 0$ V is initially applied to a Co top electrode to switch the cell of Co/ZnO/Fe from the HRS to the LRS, where a compliance current of 1 mA is used to protect the device from a permanent breakdown. Multiple sharp jumps are observed around 6 V in the corresponding *I-V* curve, as plotted in fig. 1(d), indicating the formation of multiple conductive filaments which may originate from oxygen vacancy filaments and Co conductive filaments [25,26]. To further confirm the physical properties of the filaments, the temperature dependence of resistance for the cell in the LRS is measured in the range from 10 to 300 K, as plotted in the inset of fig. 1(d). The resistance monotonously increases with temperature, showing a metallic conductive behaviour. These transport features are different from the previous studies on Pt/Co:ZnO/Pt [20] and TiN/ZnO/Pt [27], in which a semi-conductive behaviour in the LRS suggests a RS mechanism of oxygen-vacancy conductive filaments. The *R-T* curve for the cell of Co/ZnO/Fe in the LRS can be

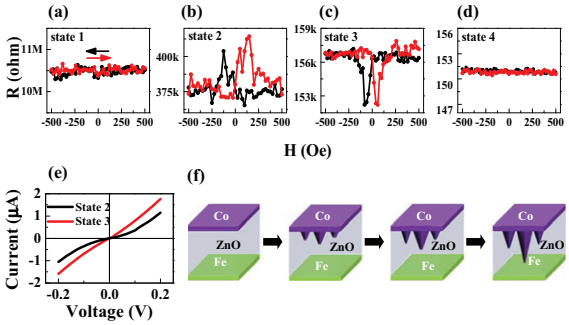

Fig. 2: (Colour on-line) The magnetoresistance curves of a Co/ZnO/Fe cell measured in (a) state 1, (b) state 2, (c) state 3, and (d) state 4. During the measurements, the magnetic field is aligned parallel to the film surface. (e) I-V curves measured for the cell in states 2 and 3. (f) Schematic of the corresponding Co/ZnO/Fe structures during the formation of Co conductive filaments.

fitted by a relation $R(T) = R_0[1 + \alpha(T - T_0)]$, where R_0 is the reference resistance at a temperature of T_0, and α is the temperature coefficient of resistance. Using $T_0 = 300\,\mathrm{K}$, α is calculated to be $8.6 \times 10^{-4}\,\mathrm{K}^{-1}$, which is in agreement with the previous study of Co nanowires grown by the focused-electron-beam–induced deposition [28]. Therefore, although we cannot completely rule out the existence of oxygen vacancy filaments, we believe that the formation of Co conductive filaments should take the most responsibility for the occurrence of RS in the Co/ZnO/Fe devices.

If the growth of Co conductive filaments can be well controlled not in contact with the Fe cathode and the ZnO barrier in between is reduced to be thin enough, we may obtain nanoscale MTJs with both Co conductive filaments and Fe layer as the electrodes. The compliance currents during voltage sweeps are applied to control the diameter and the length of conductive filaments [29]. In the present work, in order to control the growth of Co filaments, the voltage sweeps with a low compliance current in the order of 0.1 mA are performed. Meanwhile, the electrical transport properties of Co/ZnO/Fe devices in different growth states of Co filaments are systemically investigated with a magnetic field applied in the plane of films. In the as-grown state 1, the insulating ZnO barrier between Co and Fe electrodes is 100 nm in thickness, which is too long for the spin-polarized tunneling of conduction electrons, thus the TMR effect cannot be observed, as shown in fig. 2(a). After applying several (typically five to six, which are different from sample to sample) voltage sweeps of $0 \to 5 \to 0\,\mathrm{V}$ with a compliance current of 0.1 mA on Co electrodes, the devices are switched from the HRS of ten million Ω to a low-resistance state 2 of hundreds of thousands Ω. It is well known that the conductance for a point contact of Co or Fe is close to or larger than a conductance quantum, $1\,\mathrm{G}_0 = 2e^2/h \approx 1/12900\,\Omega^{-1}$, where e is the charge of electron and h is Planck's constant [30,31]. The resistance far larger than 12900 Ω indicates that none of the Co filaments is grown to reach the Fe cathode in state 2, which is also confirmed by the corresponding nonlinear I-V characteristic, as plotted in fig. 2(e). On the other hand, the ZnO barrier between Co filaments and Fe layer becomes thin enough due to the formation of Co conductive filaments, which results in the occurrence of spin-polarized electron tunneling between two ferromagnetic electrodes. Such a nanoscale Co/ZnO/Fe MTJ exhibits a smaller (larger) resistance when the two electrodes are in parallel (anti-parallel) magnetic configurations under high (low) magnetic field, corresponding to a positive TMR of 11.5% measured at a bias of −0.05 V, as shown in fig. 2(b). The TMR ratio is defined as $(R_{\mathrm{AP}} - R_{\mathrm{P}})/R_{\mathrm{P}}$, where R_{P} and R_{AP} represent the resistance with the magnetizations of two ferromagnetic layers parallel and anti-parallel to each other, respectively. Three to four additional voltage sweeps of $0 \to 5 \to 0\,\mathrm{V}$ with a compliance current of 0.1 mA are subsequently performed until the resistance of the cell is further decreased to a low-resistance state 3 of about 150 kΩ. As compared to state 2, the nonlinearity of the I-V characteristic becomes much weaker in state 3, as shown in fig. 2(e), indicating that the insulating ZnO barrier between Co filaments and Fe bottom electrode becomes even thinner. Since both Co and Fe possess a positive spin polarization, based on Jullière's model, only positive TMR could be observed in this structure [32,33]. However, in state 3 a negative TMR of about −3% is observed at a bias of −0.05 V, as shown in fig. 2(c). Finally, after further applying two or three voltage sweeps of $0 \to 6 \to 0\,\mathrm{V}$ with a compliance current of 0.15 mA, where the larger voltage and compliance current are used to accelerate the growth of Co filaments, the resistance of the cell is decreased to a small value of about 150 Ω in state 4. Consequently, the TMR effect can no more be observed in the devices, as shown in fig. 2(d), which suggests that at least one Co conductive filament has connected the two ferromagnetic electrodes in state 4. It should be noted that although there may exist more than one Co filament in the insulating ZnO matrix, the resistance and TMR of the cell are largely determined by that filament which is the closest to the Fe electrode. Figure 2(f) schematically illustrates the growth of Co conductive filaments in different states.

In order to clarify the origin of the sign change of TMR occurring in the nano-MTJs, the magnetoresistance curves of states 2 and 3 are measured at different bias voltages ranging from −0.2 to 0.2 V. For state 2, only positive TMR are observed in the whole range of measuring bias voltage, the TMR shows a maximum of 18.7% at 0.02 V and decreases to 4% and 5.8% with increasing bias voltage to 0.2 and −0.2 V, respectively. In contrast, a sign inversion of TMR is observed in state 3 by changing the measuring bias voltage, as typically plotted in fig. 3(a). The magnitude of TMR as a function of the bias voltage is summarized in fig. 3(b). When the applied bias voltage is changed from −0.2 to −0.05 V, the TMR varies from −1.5% to −2.8%. With increasing bias

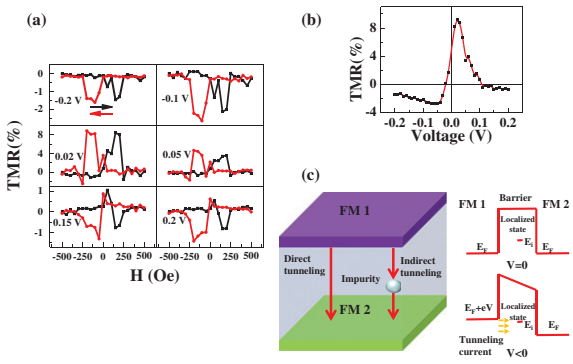

Fig. 3: (Colour on-line) (a) TMR curves for a Co/ZnO/Fe cell measured in state 3 at different bias voltages. (b) TMR ratio as a function of the bias voltage for the cell in state 3. The black dots represent the experimental data and the black solid line is a guide to the eye. The red solid line represents the numerical calculations based on the model of resonant tunneling via an impurity state located in the barrier. (c) Schematic of tunneling effect in the junction with a local impurity existing in the barrier.

voltage, the TMR ascends rapidly to positive at $-0.02\,\mathrm{V}$, and reaches its maximum value of 9.2% at 0.02 V. The TMR keeps positive and decreases monotonously when the bias voltage is varied from 0.03 to 0.1 V, and finally changes to negative values from -0.43% to -0.83% in the bias range from 0.11 to 0.2 V. The sign change of TMR with varying bias voltages has also been reported in a number of MTJs [34–38], such as Ni/NiO/Co [34] and Fe/ZnSe/Fe [37], which have been ascribed to the resonant tunneling via impurity states [34–40]. In our samples, impurity atoms and lattice defects may be introduced in the ZnO layer during the deposition of multi-layered structures and the formation of conductive filaments, giving rise to the bias-voltage–dependent impurity-resonance tunneling behaviours. When impurities are located in the ZnO barrier, resonant tunneling via the impurities occurs, which contributes to the total conductance together with the direct tunneling between Fe and Co electrodes, as shown in fig. 3(c).

For tunneling through an impurity state of energy E_i, the conductance per spin channel as a function of energy E is given by [34,39]

$$G(E) = \frac{4e^2}{h}\frac{\Gamma_1\Gamma_2}{[E - E_i - eV(1-x/d)]^2 + (\Gamma_1+\Gamma_2)^2}, \quad (1)$$

where $2\pi\Gamma_1/h$ and $2\pi\Gamma_2/h$ are leak rates of an electron from the impurity state to the Co and Fe electrodes, which are assumed for simplicity to be $\Gamma_1 \propto \rho_1 \exp(-2\kappa x)$ and $\Gamma_2 \propto \rho_2 \exp[-2\kappa(d-x)]$, where ρ_1 and ρ_2 are the densities of states of two electrodes, κ is the decay constant, x represents the position of the impurity, d is the barrier thickness and V is the bias voltage applied to the MTJ. When $|E - E_i - eV(1-x/d)| \gg \Gamma_1 + \Gamma_2$, tunneling through the impurity state leads to $G(E) \propto \rho_1\rho_2$. Due to the positive spin polarization of Fe and Co used in our multi-layered structures, a positive TMR is obtained when off resonance:

$$TMR = \frac{G_P - G_{AP}}{G_{AP}} = \frac{(\rho_{1\uparrow} - \rho_{1\downarrow})(\rho_{2\uparrow} - \rho_{2\downarrow})}{\rho_{1\uparrow}\rho_{2\downarrow} + \rho_{1\downarrow}\rho_{2\uparrow}} > 0, \quad (2)$$

where $\uparrow$ ($\downarrow$) refers to the majority (minority) spin. When $E - E_i - eV(1-x/d) = 0$, the resonant tunneling occurs between Co and Fe electrodes via the impurity state. If the impurity has an asymmetric position, $x < \mathrm{d}/2$ or $x > \mathrm{d}/2$, which leads to $\Gamma_1 \gg \Gamma_2$ or $\Gamma_1 \ll \Gamma_2$, and thus $G(E) \propto \rho_2/\rho_1$ or $G(E) \propto \rho_1/\rho_2$. In both cases, the resonant tunneling results in a negative TMR:

$$TMR = \frac{(\rho_{1\uparrow} - \rho_{1\downarrow})(\rho_{2\downarrow} - \rho_{2\uparrow})}{\rho_{1\uparrow}\rho_{2\uparrow} + \rho_{1\downarrow}\rho_{2\downarrow}} < 0. \quad (3)$$

The bias voltage dependence of TMR can be calculated by integrating eq. (1), $\int_{E_F}^{E_F+eV} G(E)\mathrm{d}E$. For simplicity, the densities of states of the two electrodes are assumed to be energy-independent constants. By using the spin polarizations of Co and Fe [41], $E_i = 35\,\mathrm{meV}$, $x = 0.35\mathrm{d}$, $\Gamma_{1\uparrow} = 6\,\mathrm{meV}$ and $\Gamma_{2\uparrow} = 70\,\mathrm{meV}$, the experimental TMR ratio as a function of the bias voltage in state 3 can be well reproduced, as shown in fig. 3(b). Since our numerical calculations only consider a single impurity state by using a simplified model, a deviation between the calculated and the experimental values cannot be avoided. To achieve a perfect agreement between theory and experiment, more factors, such as multiple impurities, the energy-dependent densities of states, and the contribution of direct tunneling, should be considered in the model.

In our nano-MTJs, the resonant tunneling strongly depends on the concentration and distribution of impurities located in the tunneling barrier [40], which results in the different TMR behaviours in states 2 and 3. To observe the inversion of TMR, two conditions need to be satisfied: the energy of a localized state lies close to the Fermi energy and the resonant tunneling overwhelms the direct tunneling between two electrodes. Theoretical calculations indicate that only the resonant tunneling through the impurities located in the middle region of the barrier makes a considerable contribution to the total conductance. The high concentration of impurities is another determinant for the appearance of a strong resonance signal [39,40]. Therefore, due to the different configurations of impurities in different MTJs, there is only a finite probability to observe the inversion of TMR, which has been proved in Ni/NiO/Co nano-junctions by Tsymbal *et al.* [34]. For our Co/ZnO/Fe junctions, with continuously performing voltage sweeps, Co ions keep migrating into the ZnO barrier, and become new impurities. As a result, the high concentration of defect atoms in the ZnO barrier enhances the contribution of resonant tunneling and leads to the occurrence of the inversion of TMR.

Summary and conclusion. – In summary, we have systematically studied the magnetotransport behaviours

of the Co/ZnO/Fe sandwich structures in different RS states. The formation of Co conductive filaments in a ZnO layer under the application of voltage sweeps can be employed to effectively produce nanoscale MTJs and control the magnetic transport. The pristine Co/ZnO/Fe sandwich structure with a 100 nm thick ZnO layer does not exhibit any TMR behaviour. By applying a positive voltage on Co electrodes, Co atoms migrate into the insulating ZnO layer, forming conductive filaments. When the Co conductive filaments are close enough to the Fe cathode after the execution of electrical operations, a positive TMR can be observed, indicating formation of nanoscale Co/ZnO/Fe MTJs. In addition, the negative TMR and the sign change of TMR with varying bias voltages are observed after further electrical operations have been carried on to change the effective ZnO barrier. The anomalous TMR behaviours can be well understood in terms of resonant tunneling caused by the impurity scattering.

* * *

The authors acknowledge the financial support from the National Natural Foundation of China (11174302, 11374312), State Key Project of Fundamental Research of China (2012CB933004), and Ningbo Science and Technology Innovation Team (2011B82004).

REFERENCES

[1] Liu S. Q., Wu N. J. and Ignatiev A., *Appl. Phys. Lett.*, **76** (2000) 2749.
[2] Waser R. and Aono M., *Nat. Mater.*, **6** (2007) 833.
[3] Miyazaki T. and Tezuka N., *J. Magn. & Magn. Mater.*, **139** (1995) L231.
[4] Moodera J. S., Kinder L. R., Wong T. M. and Meservey R., *Phys. Rev. Lett.*, **74** (1995) 3273.
[5] Yuasa S., Nagahama T., Fukushima A., Suzuki Y. and Ando K., *Nat. Mater.*, **3** (2004) 868.
[6] Parkin S. S. P., Kaiser C., Panchula A., Rice P. M., Hughes B., Samant M. and Yang S. H., *Nat. Mater.*, **3** (2004) 862.
[7] Baibich M. N., Broto J. M., Fert A., Van Dau F. N., Petroff F., Etienne P., Creuzet G., Friederich A. and Chazelas J., *Phys. Rev. Lett.*, **61** (1988) 2472.
[8] Binasch G., Grunberg P., Saurenbach F. and Zinn W., *Phys. Rev. B*, **39** (1989) 4828.
[9] Parkin S. S. P., More N. and Roche K. P., *Phys. Rev. Lett.*, **64** (1990) 2304.
[10] Kim K. M., Jeong D. S. and Hwang C. S., *Nanotechnology*, **22** (2011) 254002.
[11] Pan F., Gao S., Chen C., Song C. and Zeng F., *Mater. Sci. Eng. R*, **83** (2014) 1.
[12] Waser R., Dittmann R., Staikov G. and Szot K., *Adv. Mater.*, **21** (2009) 2632.
[13] Xiong Z. H., Wu D., Vardeny Z. V. and Shi J., *Nature*, **427** (2004) 821.
[14] Yuasa S., Nagahama T. and Suzuki Y., *Science*, **297** (2002) 234.
[15] Karnaushenko D., Makarov D., Yan C., Streubel R. and Schmidt O. G., *Adv. Mater.*, **24** (2012) 4518.
[16] Garcia V., Bibes M., Bocher L., Valencia S., Kronast F., Crassous A., Moya X., Enouz-Vedrenne S., Gloter A., Imhoff D., Deranlot C., Mathur N. D., Fusil S., Bouzehouane K. and Barthélémy A., *Science*, **327** (2010) 1206.
[17] Pantel D., Goetze S., Hesse D. and Alexe M., *Nat. Mater.*, **11** (2012) 289.
[18] Prezioso M., Riminucci A., Bergenti I., Graziosi P., Brunel D. and Dediu V. A., *Adv. Mater.*, **23** (2011) 1371.
[19] Krzysteczko P., Reiss G. and Thomas A., *Appl. Phys. Lett.*, **95** (2009) 112508.
[20] Chen G., Song C., Chen C., Gao S., Zeng F. and Pan F., *Adv. Mater.*, **24** (2012) 3315.
[21] Halley D., Majjad H., Bowen M., Najjari N., Henry Y., Ulhaq-Bouillet C., Weber W., Bertoni G., Verbeeck J. and Van Tendeloo G., *Appl. Phys. Lett.*, **92** (2008) 212105.
[22] Jang H. J., Kirillov O. A., Jurchescu O. D. and Richter C. A., *Appl. Phys. Lett.*, **100** (2012) 043510.
[23] Liu Q., Sun J., Lv H. B., Long S. B., Yin K. B., Wan N., Li Y. T., Sun L. T. and Liu M., *Adv. Mater.*, **24** (2012) 1844.
[24] Peng S. S., Zhuge F., Chen X. X., Zhu X. J., Hu B. L., Pan L., Chen B. and Li R. W., *Appl. Phys. Lett.*, **100** (2012) 072101.
[25] Liu Q., Dou C. M., Wang Y., Long S. B., Wang W., Liu M., Zhang M. H. and Chen J. N., *Appl. Phys. Lett.*, **95** (2009) 023501.
[26] Yang Y. C., Chen C., Zeng F. and Pan F., *J. Appl. Phys.*, **107** (2010) 093701.
[27] Xu N., Liu L., Sun X., Liu X. W., Han D. D., Wang Y., Han R. Q., Kang J. F. and Yu B., *Appl. Phys. Lett.*, **92** (2008) 232112.
[28] Fernández-Pacheco A., De Teresa J. M., Córdoba R. and Ibarra M. R., *J. Phys. D: Appl. Phys.*, **42** (2009) 055005. The temperature coefficient of resistance of Co nanowire reported by this reference is about $9 \times 10^{-4}\,\mathrm{K}^{-1}$ (calculated from the resistivity-temperature relationship depicted in fig. 2 of this reference).
[29] Zhu X. J., Su W. J., Liu Y. W., Hu B. L., Pan L., Lu W., Zhang J. D. and Li R. W., *Adv. Mater.*, **24** (2012) 3941.
[30] Egle S., Bacca C., Pernau H. F., Huefner M., Hinzke D., Nowak U. and Scheer E., *Phys. Rev. B*, **81** (2010) 134402.
[31] Calvo M. R., Fernandez-Rossier J., Palacios J. J., Jacob D., Natelson D. and Untiedt C., *Nature*, **458** (2009) 1150.
[32] Julliere M., *Phys. Lett. A*, **54** (1975) 225.
[33] Maekawa S. and Gafvert U., *IEEE Trans. Magn.*, **18** (1982) 707.
[34] Tsymbal E. Y., Sokolov A., Sabirianov I. F. and Doudin B., *Phys. Rev. Lett.*, **90** (2003) 186602.
[35] Beaufrand J. B., Dayen J. F., Kemp N. T., Sokolov A. and Doudin B., *Appl. Phys. Lett.*, **98** (2011) 142504.
[36] Sokolov A., Sabirianov R., Sabirianov I. and Doudin B., *J. Phys.: Condens. Matter*, **21** (2009) 485303.

[37] Varalda J., de Oliveira A. J. A., Mosca D. H., George J. M., Eddrief M., Marangolo M. and Etgens V. H., *Phys. Rev. B*, **72** (2005) 081302(R).
[38] Garcia V., Jaffrès H., Eddrief M., Marangolo M., Etgens V. H. and George J. M., *Phys. Rev. B*, **72** (2005) 081303(R).
[39] Ren Y., Li Z. Z., Xiao M. W. and Hu A., *Phys. Rev. B*, **75** (2007) 054420.
[40] Sheng L., Xing D. Y. and Sheng D. N., *Phys. Rev. B*, **69** (2004) 132414.
[41] Tedrow P. M. and Meservey R., *Phys. Rev. B*, **7** (1973) 318.